eng

MDPI

Article

Study of the Effect of an Environmentally Friendly Flood Risk Reduction Approach on the Oman Coastlines during the Gonu Tropical Cyclone (Case Study: The Coastline of Sur)

Masoud Banan-Dallalian [1,*], Mehrdad Shokatian-Beiragh [1,*], Aliasghar Golshani [2], Alireza Mojtahedi [1], Mohammad Ali Lotfollahi-Yaghin [1] and Shatirah Akib [3]

[1] Deptartment of Water Resources Eng, Faculty of Civil Engineering, University of Tabriz, Tabriz 5166616471, Iran; a.mojtahed@tabrizu.ac.ir (A.M.); lotfollahi@tabrizu.ac.ir (M.A.L.-Y.)
[2] Department of Civil Engineering, Islamic Azad University, Central Tehran Branch, Tehran 13117773591, Iran; ali.golshani@iauctb.ac.ir
[3] Department of Civil Engineering, School of Architecture, Design and the Built Environment, Nottingham Trent University, Nottingham NG1 4FQ, UK; shatirah.akib@ntu.ac.uk
* Correspondence: masoud.banan92@ms.tabrizu.ac.ir (M.B.-D.); m.shokatian.b92@ms.tabrizu.ac.ir (M.S.-B.)

Abstract: Tropical cyclones may be destructive in the coastal region, such as the Gonu tropical cyclone, which affected the Arabian Peninsula and parts of southern Iran in 2007. In this study, a coupled MIKE 21/3 HD/SW (hydrodynamic/spectral wave) model was used to simulate the inland flooding inside the Sur port during the Gonu tropical cyclone. The MIKE 21 Cyclone Wind Generation (CWG) tool was utilized to generate the cyclone's wind and pressure field. The required input data were obtained from the International Best Track Archive for Climate Stewardship (IBTrACS) and imported into the CWG tool. In this study, the wind and pressure fields were compared between the analytical vortex model and European Centre for Medium-Range Weather Forecasts (ECMWF) data during the Gonu cyclone passage. Moreover, by developing a new model, artificial Mangroves' effect on inland flooding was investigated. The results show that, contrary to the ECMWF data, the analytical vortex models well captured the storm event's wind and pressure field. Furthermore, the flood hazard is calculated based on the inundation depth, flow velocity, and area's vulnerability. The flood hazard map shows that 5% of the coast is at high-risk, 49% is at medium-risk, and 46% is at low-risk class in the Sur port. By applying Mangroves as flood risk reduction, the high-risk area is almost completely removed. However, medium and low-risk zones increase by 50% and 50%, respectively. This information could be helpful in disaster risk reduction and coastal management in the future.

Keywords: flood hazard; risk; Gonu tropical cyclone; Sur; mangroves

Citation: Banan-Dallalian, M.; Shokatian-Beiragh, M.; Golshani, A.; Mojtahedi, A.; Lotfollahi-Yaghin, M.A.; Akib, S. Study of the Effect of an Environmentally Friendly Flood Risk Reduction Approach on the Oman Coastlines during the Gonu Tropical Cyclone (Case Study: The Coastline of Sur). *Eng* **2021**, *2*, 141–155. https://doi.org/10.3390/eng2020010

Academic Editor: Antonio Gil Bravo

Received: 7 January 2021
Accepted: 7 April 2021
Published: 15 April 2021

1. Introduction

The storm hazards impact the coastal zones. These extreme conditions may cause damage to the coastal facilities and human life [1,2]. Many communities are located in the coastal area and comprise a large amount of population. Hence, these communities are commercial hubs and industrial activities centers and are valuable areas [3,4].

Due to the increasing global temperature, the severity and the frequency of tropical cyclones in the oceans have increased since 1970 [5]. Based on the statistics, there are over 80 tropical cyclones worldwide annually [6]. The tropical cyclones in the Atlantic and Eastern Pacific Oceans are known as Hurricane, the Western Pacific Ocean as Typhoon and the Indian Ocean and the Arabian Sea as Cyclone [7]. After forming the cyclones in the Arabian Sea, they mostly move toward the south and southeast Oman, west India, and south Pakistan and rarely enter the Oman Sea [8]. However, these cyclones can move different paths, affecting the coasts of countries such as Iran and even the United Arab

Emirates [9]. The Gonu cyclone has been the strongest cyclone ever formed in the Arabian Sea, influencing the Arabian Peninsula and parts of southern Iran from 2 June 2007 to 7 June 2007 (Figure 1). It killed 49 people on the coast of Oman and 23 people on the south coast of Iran. In addition, the financial damage done by this storm is estimated to be $4 billion in Oman and about $215 million in Iran [10]. Therefore, investigating cyclones' consequences and their modelling to determine the most hazardous zone on the coasts for future management and planning are critical issues. Besides, evaluating the impact of the storms that occurred in Iran's neighboring countries greatly helps manage the future storm crisis due to the random nature of the storm tracks and the lack of measured data. Regarding the vulnerability of sandy beaches against flooding, overwash, and erosion, the present study aims to evaluate the impact of inland flooding by Gonu cyclone on the coastline of Sur.

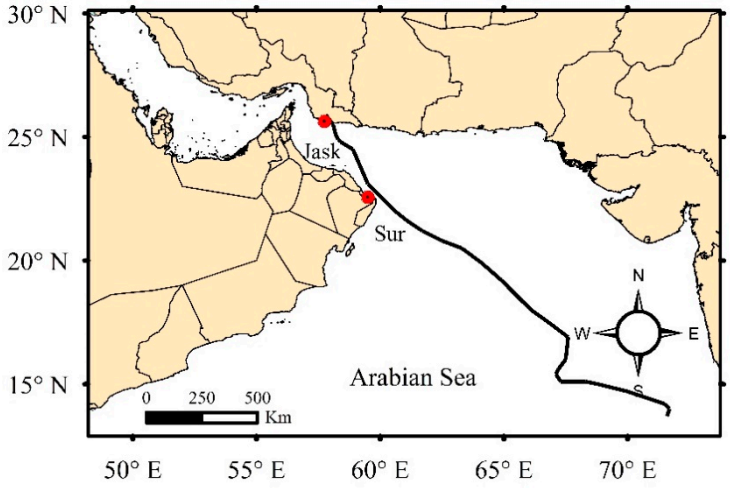

Figure 1. The Gonu cyclone track.

Khaniki et al., simulated the characteristic wave height of six tropical storms in the Indian Ocean [11]. Dibajnia et al., evaluated the maximum wave height simulation from the 1889's Gonu cyclone in the Arabian Sea [8]. Fritz et al. assessed the depth of the flood by Gonu cyclone in some affected ports of Oman including the Sur port, as a field study [10]. Mashhadi et al., used a third-generation SWAN model for modelling the Gonu cyclone and compared the numerical results through a buoy in the Chabahar port [12]. Bakhtiari et al., simulated the recent storms that occurred in the Arabian Sea, such as the Gonu cyclone, through the two-dimensional MIKE 21 model and compared the results of the hydrodynamic and wave models with the measured data in the Oman Gulf [13]. Other research studies have been conducted to evaluate the oceanographic responses to Gonu tropical cyclone and Wave pattern generated [14–17].

The previous studies and modelling concentrated more on evaluation and predicting the effects of offshore storms. However, increasing the wave height may affect coasts and land areas as well as offshore locations. The Gonu cyclone caused some flooding by the storm surge in some parts of the Oman coast, including Muscat, Qirat, Sur, and Ras al-Hadd. The flood damage in Sur port was significant in which approximately 4294 residential homes were damaged [18]. The flooding hazard assessment for Sur port and understanding how the Gonu cyclone proved to be such a destructive event are the purposes of this study. This information could be helpful in disaster risk reduction. In this study, the flood caused by the Gonu cyclone in the coastal part of Sur port was modelled by MIKE 21 modelling software. Meanwhile, artificial Mangroves' effect as an environmentally friendly flood-risk-reduction approach on the coastlines of Sur was investigated during the Gonu tropical cyclone. For this purpose, the impact of Mangroves on coastal inland flooding was considered. Further, the results of a bigger model related to the monitoring

and modelling of the Makran Coastline project [19] were used to define the existing smaller model's boundary conditions.

This study's main objectives are to investigate the risk of flood due to the Gonu cyclone and identify vulnerable areas in the Sur port. This information can help the managers and governments for coastal planning and management in the future. Moreover, the effect of using an environmentally friendly method to mitigate the destructive influences of cyclones is another goal of this study.

2. Case Study

Historically, the Sur is known for being an important destination point for sailors. Today, the sea still plays an integral part in Sur's life. The port has a lagoon, and it is protected by rubble mound breakwater (Figure 1). In this port, a considerable portion of the population inhabits the coastal areas or is engaged in commercial and recreational activities. Therefore, the storm can cause a lot of loss of life and economic damage to the port's inhabitants. The considered area is shown in Figure 2a, and the dominant direction of the waves in this area during the cyclone is from the east and south-west, and the offshore wave height could reach up to 9 m.

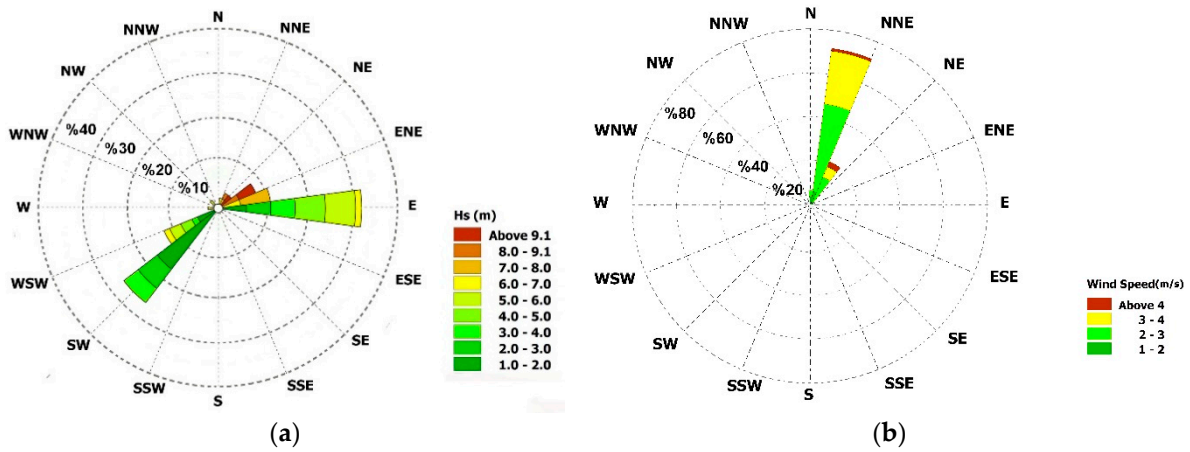

(**a**) (**b**)

Figure 2. (**a**) Wave rose for Sur port during the Gonu cyclone extracted from Makran model. (**b**) Monthly means of daily average wind data for the Sur port station for the period of 1981–2019 during the Kharif season.

Most of the tropical cyclones in the Arabian Sea are formed in pre-monsoon (May) and post-monsoon seasons (October and November) [20]. However, some cyclones are formed between June to early September (Kharif season). The Kharif season monthly means of daily average wind data for the Sur port station were obtained from European Centre for Medium-Range Weather Forecasts (ECMWF) reanalysis of the ERA-interim data from 1981 to 2019 (Figure 2b). As shown in the Kharif season, the wind speed increased and reached up to 4 m/s, and the northeast is the dominant wind direction in the Sur port.

3. Materials and Methods

3.1. The Governing Equation of MIKE21 SW

The basis of the MIKE 21 SW model for wave prediction is to solve the energy transfer equation along with the source and sink terms. The energy transfer equation is considered in its spectral form to account for the random sea wave nature.

The wave model's governing equation is based on a wave action density spectrum N(σ,θ), defined in Equation (1).

$$\mathrm{N}(\sigma,\ \theta) = \frac{E}{\sigma}, \tag{1}$$

where σ is the independent phase parameter (the relative angular frequency), and θ is the wave propagation direction. E is the energy density [21].

MIKE 21 SW includes directional decoupling and full spectral of formulations. Parameterisation is performed in a frequency range by inputting the zero moment and the wave action spectrum's first momentum as parameters. The wave action balance equation is formulated in Cartesian or spherical coordinates (Equation (2)).

$$\frac{E}{\sigma} = \frac{\partial N}{\partial t} + \nabla.(\overline{v}N) = \frac{S}{\sigma'}, \tag{2}$$

where $N(\overline{x}, \sigma, \theta, t)$ is the action density, t is the time, $\overline{x} = (x, y)$ are the Cartesian coordinates, and $\overline{v}(C_x, C_y, C_\sigma, C_\theta)$ is the propagation velocity of a wave group in the four-dimensional phase space of x, σ, and θ. S is the source term for the energy balance equation, and ∇ is the four-dimensional differential operator in the x, σ, and θ space. In this present study, the full spectral formulation was chosen.

3.2. The Governing Equation of MIKE21 FM

The hydrodynamic model of MIKE 21 FM is based on the numerical solution of the two dimensional incompressible Reynolds averaged Navier-Stokes equations summoning the assumptions of Boussinesq and hydrostatic pressure [22].

The continuity equation in Cartesian coordinates is in the form of Equation (3).

$$\frac{\partial h}{\partial t} + \frac{\partial h\overline{u}}{\partial x} + \frac{\partial h\overline{v}}{\partial y} = hs, \tag{3}$$

The horizontal momentum shallow water equations in Cartesian coordinates is expressed as Equations (4) and (5).

$$\frac{\partial h\overline{u}}{\partial t} + \frac{\partial h\overline{u}^2}{\partial x} + \frac{\partial h\overline{v}\overline{u}}{\partial y} = f\overline{v}h - gh\frac{\partial \eta}{\partial x} - \frac{h}{\rho_0}\frac{\partial p_a}{\partial x} - \frac{gh^2}{2\rho_0}\frac{\partial \rho}{\partial x} + \frac{\tau_{sx}}{\rho_0} - \frac{\tau_{bx}}{\rho_0} - \frac{1}{\rho_0}\left(\frac{\partial s_{xx}}{\partial x} + \frac{\partial s_{xy}}{\partial y}\right) + \frac{\partial}{\partial x}(hT_{xx}) + \frac{\partial}{\partial x}(hT_{xy}) + hu_sS \tag{4}$$

$$\frac{\partial h\overline{v}}{\partial t} + \frac{\partial h\overline{u}\overline{v}}{\partial x} + \frac{\partial h\overline{v}^2}{\partial y} = -f\overline{u}h - gh\frac{\partial \eta}{\partial y} - \frac{h}{\rho_0}\frac{\partial p_a}{\partial y} - \frac{gh^2}{2\rho_0}\frac{\partial \rho}{\partial y} + \frac{\tau_{sy}}{\rho_0} - \frac{\tau_{by}}{\rho_0} - \frac{1}{\rho_0}\left(\frac{\partial s_{yx}}{\partial x} + \frac{\partial s_{yy}}{\partial y}\right) + \frac{\partial}{\partial x}(hT_{xy}) + \frac{\partial}{\partial y}(hT_{yy}) + hv_sS \tag{5}$$

The parameters in Equations (4) and (5) are described in Table 1.

Table 1. Description of the parameters in Equations (4) and (5).

Parameter	Description	Unit
u, v	Depth average velocity components in the x, y direction	m/s
S	Magnitude of the discharge due to point sources	-
h	Total water depth	m
η	Surface elevation	m
t	Time	s
x, y	Cartesian coordinates	m
f	Coriolis parameter	s^{-1}
g	Gravitational acceleration	m/s^2
ρ_0	Reference density of water	kg/m^3
p_a	Atmospheric pressure	$kg/m/s^2$
ρ	Density of water	kg/m^3
$\tau_{sx}, \tau_{sy}, \tau_{bx}, \tau_{by}$	Components of the surface wind and bottom stress	kg/m^2
$s_{xx}, s_{xy}, s_{yx}, s_{yy}$	Components of the surface wind and bottom stress	kg/m^2
T_{xx}, T_{xy}, T_{yy}	Lateral stresses	kg/m^2
v_s	Velocity by which the water is discharged into the ambient water	m/s

3.3. Data and Modeling

The data are used to model the coastal flood caused by the Gono cyclone in the Sur port including wind, bathymetry, and water level. The data were obtained using the available international databases, which are given in Table 2.

Table 2. The input calibration datasets.

		Input Datasets	Calibration Datasets
Wind		International Best Track Archive for Climate Stewardship (IBTrACS) datasets, (http://ibtracs.unca.edu/, accessed date: 7 March 2020)	European Centre for Medium-Range Weather Forecasts (ECMWF) datasets, (https://www.ecmwf.int/, accessed date: 10 April 2020)
			Jask synoptic station
Topographic	Bathymetry	General Bathymetric Chart of the Ocean (GEBCO) datasets, (https://www.gebco.net/, accessed date: 22 April 2020)	-
	Hypsometry	United States Geological Survey (USGS) datasets, (https://www.usgs.gov/, accessed date: 22 April 2020)	
Water level		Study reports of Monitoring and Modelling Studies of Markan Coastlines [19]	HYbrid Coordinate Ocean Model (HYCOM) datasets, (https://www.hycom.org/, accessed date: 29 May 2020)

One of the principal constituents for the modelling in storm condition is the precise wind and pressure field because the wind and pressure cause shear stresses, which made surge current and wave [23,24]. If the available wind fields cannot capture the cyclone wind fields or wind data are not available at all, then the charts of atmospheric surface pressure can be used [25].

In this study, the MIKE 21 Cyclone Wind Generation (CWG) tool (Danish Hydraulic Institute (India), dhigroup.com, Headquarters location: Hørsholm, Denmark, Founded: 1964, Parent organization: DHI Water & Environment) was utilized to generate the cyclone's wind and pressure field. The Young and Sobey (1981), Holland (1980), and Rankine (1872) vortex models were used to generate the wind and pressure fields during the passage of the Gonu cyclone [26–28]. Cyclone position, central pressure, maximum sustained wind speed, and radius to the maximum wind (R_{Vmax}) are the model's requirement input data [25]. International Best Track Archive for Climate Stewardship (IBTrACS) global tropical cyclone database has been used to obtain these data. The results were compared with observed wind and pressure data obtained from 3 hourly Jask meteorology synoptic station and the ECMWF reanalysis ERA5 data. ERA5 has a special resolution of 0.25° and a temporal resolution of an hour. The wind and pressure field modelled using the CWG tool was validated using available data from the Jask meteorological synoptic Station. Due to the Gonu cyclone track's proximity to the Jask station (about 16 km), the ECMWF ERA5 could not capture the cyclone wind and pressure fields. However, ERA5 is accurate enough in non-cyclonic weather conditions. The analytical vortex models well captured the wind and pressure field during cyclone passage from the study area (Figure 3).

For the statistical analysis of the dimensionless goodness-of-fit indicator, the Nash and Sutcliffe coefficient of efficiency is calculated as follows [29]:

$$NSE = 1 - \frac{\sum_{i=1}^{N}(O_i - P_i)^2}{\sum_{i=1}^{N}(O_i - \overline{O})^2} = 1 - \left(\frac{RMSE}{SD}\right)^2, \quad (6)$$

where, O_i and P_i represent the sample (of size N) containing the observations and the simulation, respectively. $\overline{O}$ is the mean of the observed values SD represents the standard deviation of the observation data, and the root mean square error ($RMSE$) is given by Equation (7):

$$RMSE = \sqrt{\frac{\sum_{i=1}^{N}(O_i - P_i)^2}{N}}. \quad (7)$$

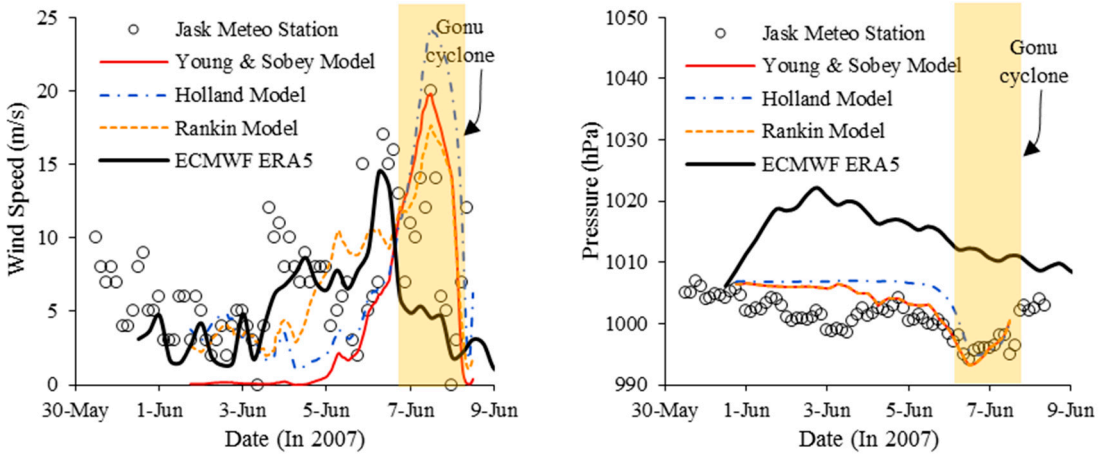

Figure 3. Comparison of the (**a**) wind and (**b**) pressure data from the analytical vortex models and ECMWF ERA5 at Jask synoptic station during Gonu cyclone.

Ritter and Munoz-Carpena proposed four model performance classes based on *NSE* ranges (Table 3), denoted as Unsatisfactory, Acceptable, Good, and Very good [30].

Table 3. Criteria for the goodness-of-fit evaluation [30].

	Performance Rating			
	Very Good	**Good**	**Acceptable**	**Unsatisfactory**
NSE	≥0.90	0.80–0.90	0.65–0.80	<0.65

During the Gonu cyclone passage from the Jask synoptic station (7 June), the NSE values are 0.68, 0.66, and 0.72 for the Young and Sobey, Holland, and Rankine vortex model results, respectively. In contrast, the NSE of the ECMWF ERA5 is 0.57. According to the criteria for the goodness-of-fit evaluation (Table 3), the Young and Sobey, Holland and Rankine vortex model results' performance is "Acceptable." However, the ECMWF ERA5 data performance rating is "Unsatisfactory," while, in the normal condition, the ECMWF ERA5 data performance is "Good" (NES = 0.81).

Wind fields were extracted from the MIKE 21 CWG a grid extending from the latitudes of 22.15–24.15° N and longitudes of 59–60.45° E, from the 5–6 June 2007 (Figure 4). As shown in Figure 4, during the typhoon's passage, the MIKE 21 CWG data represented the wind field accurately within the Sur port's vicinity.

The topographic data (bathymetry and hypsometry) have been generated by merging two different datasets. The Digital Elevation Model (DEM) with 30 m spatial resolution, which could be interpolated onto the model, was created for the shore zone as hypsometry data. The bathymetry dataset was complemented by the General Bathymetric Chart of the Ocean (GEBCO). However, due to the importance of sea depth data near the shore, the study area's shore profile was modified [31]. Figure 5 shows the modification beach profile. In addition, a dfs2 file was prepared for importing into the MIKE 21 through ArcGIS in the land area. For this purpose, the raster map of the area was created through the IDW tool in ArcGIS at the elevation points. Further, the limited DEM file was available, which can be imported into MIKE 21 as region-specific data through converting it to a dfs2 file.

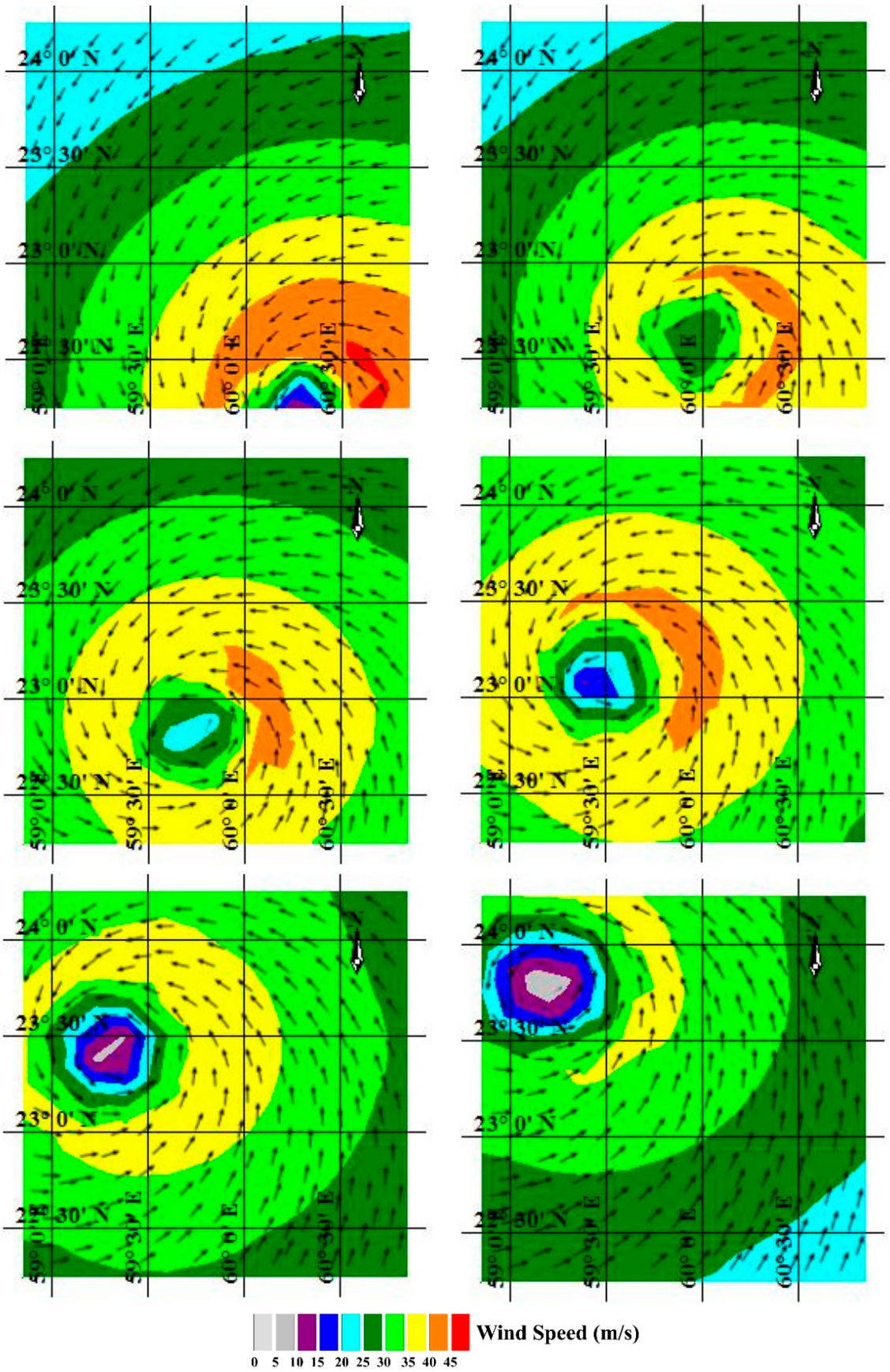

Figure 4. Extracted wind field from the MIKE 21 CWG at 3-hourly intervals from a 5 June to 09:00–12:00 p.m. 6 June.

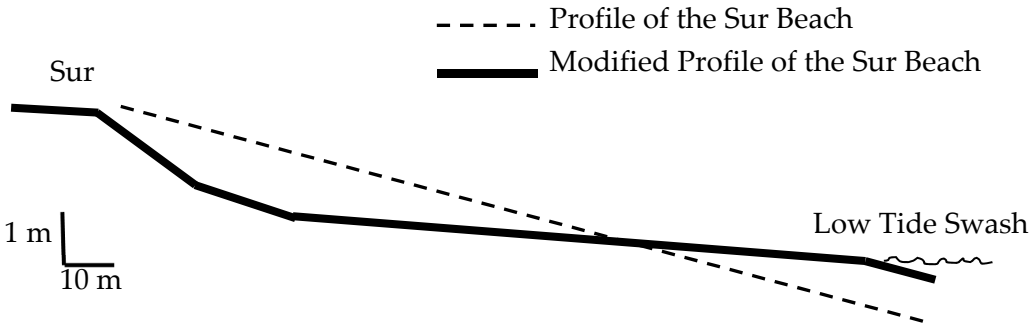

Figure 5. The profile of the Sur beach before and after modification.

The Gonu tropical cyclone formed from 2–7 June 2007. The coupled MIKE 21/3 HD/SW (hydrodynamic/spectral wave) model simulated the inundation depth and the flow velocity. The MIKE 21 simulation was performed for approximately seven days from 31 May 2007 to 7 July 2007 on the coast of Sur and for a time interval of 300 s. The model extends 14 km offshore from the case study site, over an area of 110 km^2. The unstructured mesh includes 34,515 elements with 17,606 nodes (Figure 6). The largest elements have a resolution of 0.5 km, but the grid resolution becomes more refined toward the coast, with the smallest resolutions in the Sur coastal zone of approximately 15 m.

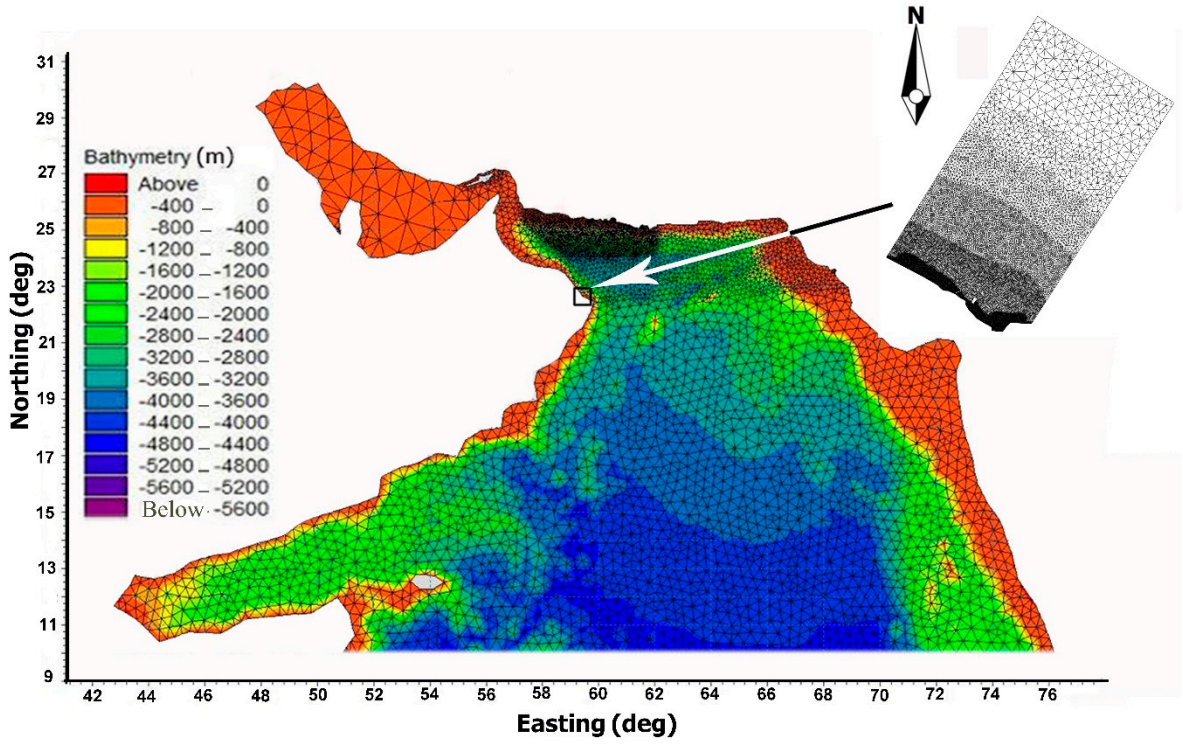

Figure 6. Computational domain and mesh used in this study.

In this study, the surface elevation was applied at the northern open boundary, while the current speed was applied at eastern and western open boundaries. The boundary conditions were extracted from Makran MIKE 21/3 coupled model, which covered the Arabian Sea and the Persian Gulf. The Young and Sobey vortex model was used to generate the wind and pressure fields in the Makran model. ECMWF ERA-Interim wave dataset with a resolution of 0.75 degree was used as wave parametric boundary condition at the open boundary located on 10° N latitude in Makran model.

HYbrid Coordinate Ocean Model (HYCOM) GOFS 3.1 database with a spatial resolution of 0.08° and temporal resolution of 3-h was used to compare with the simulated surface

elevation at the point with coordinates of 22°38′24.00″ N 59°36′0.00″ E. The calibration parameters of the MIKE 21 model were chosen based on the minimization of the error in the water level simulation. Figure 7 shows a comparison between the HYCOM GOFS 3.1 data and the simulated water level. It can be seen that the numerical result reasonably matches the HYCOM GOFS 3.1 data. The NSE value in this comparison is 0.91, and the performance rate of fit is "Very Good" (Table 3). Note that the HYCOM GOFS 3.1 water level data does not exist between the 4 June 2007 12:00 a.m. and 6 June 2007 12:00 p.m.

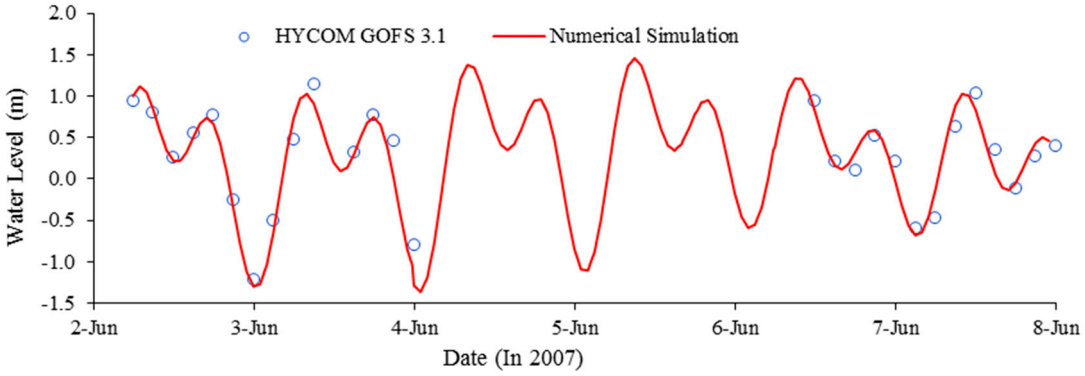

Figure 7. Comparison between the HYCOM GOFS 3.1 data and the simulated water level during the Gonu cyclone.

The Manning coefficient's determination is a challenge because of its empirical nature, and judgment and experience are needed. First of all, the parameter affecting the coefficient must be considered to select suitable values. The most crucial factors considered in the previous studies are surface roughness, vegetation, seasonality, level of water, surface irregularities, and obstructions [32]. In this study, the Manning's coefficient based on land cover data is used. The model was calibrated based on HYCOM GOFS 3.1 water level data to achieve a suitable local Manning coefficient for both open water and land area in Sur port. Table 4 shows the final Manning's coefficient values for the study areas. Meanwhile, Manning's coefficient value (n) in Table 4 is needed for inundation modelling with MIKE 21 FM. The Manning's coefficient (M) for open water in the Makran MIKE 21/3 coupled model was considered to be 60 $m^{1/3}/s^{1}$.

Table 4. Manning values for land cover classes in the Sur port to describe bottom roughness [33].

Surface Class	Manning's Coefficient (n)	Manning's Coefficient (M) in $m^{1/3}$ s^{-1}
Barren Land, Sand, Beach, Roads	0.031	32
Urban Area	0.060	17
Buildings	0.090	11
Open Sea	0.020	50

4. Results and Discussion

The flood model results caused by the Gono cyclone in the Sur port are presented in two sections. First of all, the inundation and current speed model prediction, and the other, Mangrove for flood mitigation scenario model. The mentioned sections are presented in the following.

4.1. Inundation Model Results

Gonu cyclone generated destructive storm surge at the Sur port. Figure 8 shows the Storm Surge in the Sur port during the Gonu cyclone event. As shown in Figure 8, when the cyclone passed by the considering area, the storm surge near the Sur shore achieved its peak value. Meanwhile, it seems that there are no significant differences among the results of storm surge from different analytical vortex models.

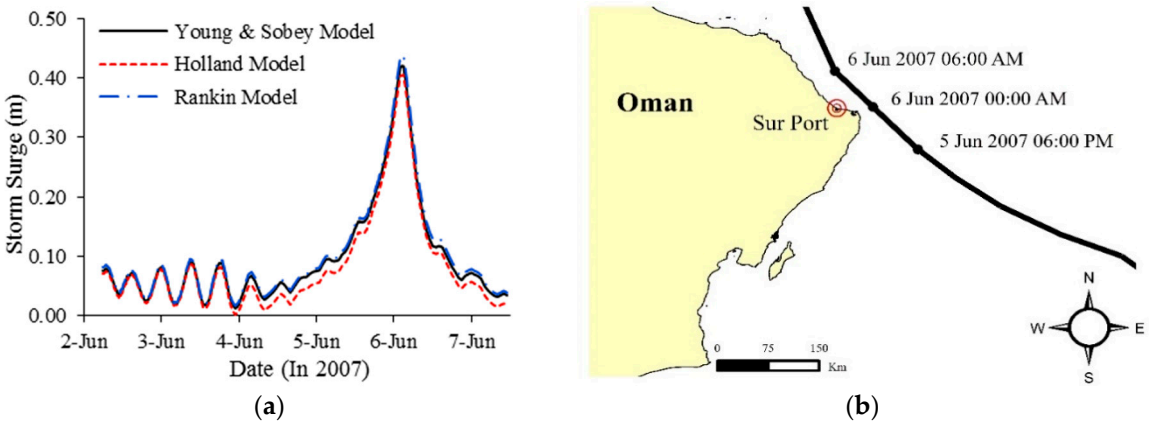

Figure 8. (**a**) Comparison of Storm surge generated by the Young and Sobey, Holland, and Rankine vortex models near the Sur shore during Gonu cyclone, (**b**) Gonu cyclone track passing by the coastline of Sur port.

Figure 9 shows the spatial map of flood characteristic for inundation depth and flow velocity. Maximum inundation depth occurs along the shoreline over the central part of the study area (Figure 9a) with values ~1.3 m. Furthermore, for most of the model's western part, the inundation depth increases up to ~1.1 m, while the maximum inundation depth in the eastern part of the model is approximately less than 1 m. The flow velocity pattern for the storm event is presented in Figure 9b. The maximum flow velocity varies all over the study area, with its maximum magnitude being more than 0.9 m/s.

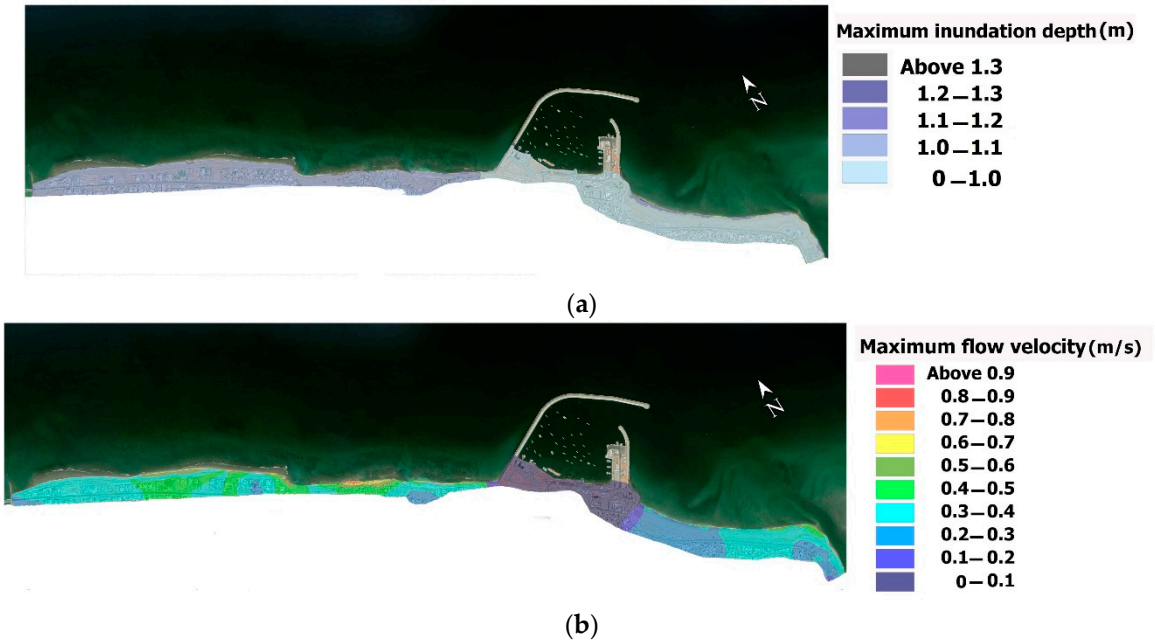

Figure 9. (**a**) Maximum inundation depth. (**b**) Maximum flow velocity in the study area according to the Gonu cyclone model.

In this study, the flood hazard is calculated through a matrix (Table 5) based on the inundation depth, flow velocity, and area's vulnerability. Vulnerability or, on the other hand, nature of the area is based on the type of buildings, the construction methods, and land-use at three levels: Low (Multi-story apartments), Medium (Typical residential area (2-storey), commercial and industrial properties), and High (Bungalows, mobile homes, busy roads, parks, single-story schools, campsites, etc.) vulnerabilities [34].

Table 5. Flood hazard matrix thresholds as a function of inundation depth and flow velocity and nature of the area.

	Nature of Area		
Inundation Depth × Flow Velocity (m^2/s)	**Low Vulnerability**	**Medium Vulnerability**	**High Vulnerability**
<0.25	Low Risk	Low Risk	Low Risk
0.25–0.50	Low Risk	Medium Risk	Medium Risk
0.50–1.10	Medium Risk	Medium Risk	High Risk
1.10–7.00	Medium Risk	High Risk	Extreme Risk
>7.00	Extreme Risk	Extreme Risk	Extreme Risk

The flood hazard map based on the literature discussed above and according to Table 5 is reported in Figure 10. As shown in Figure 10, approximately 5% of the coast is assigned to the high-risk class, 49% of Medium, and 46% of low-risk. The area with a low-risk to life is located mostly in the central and eastern parts of the model in which the breakwater is located. While the area with high-risk to life is shown in the western part of the Sur coast. The medium-risk to life zone exists in both the eastern and western parts of the coast.

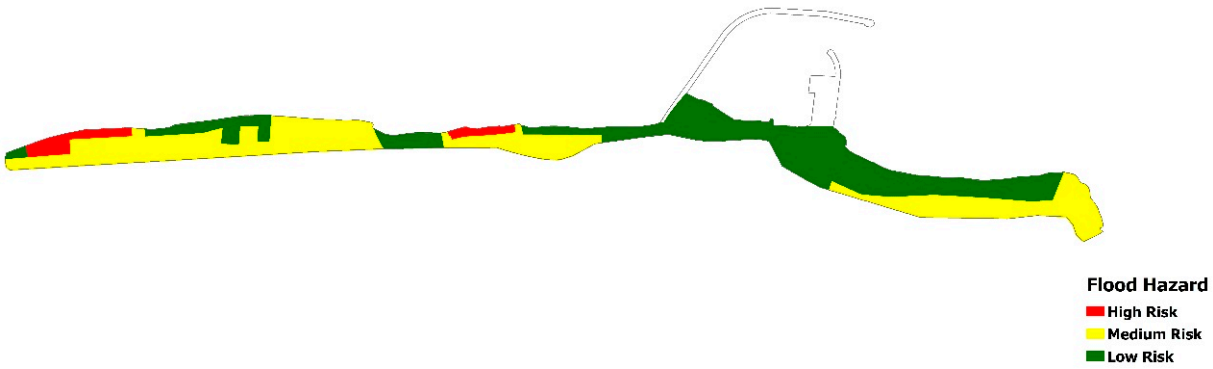

Figure 10. Flood hazard map in the study area according to the Gonu cyclone model.

4.2. Mangroves for Mitigation Scenario

Mangroves are the first line of defense against coastal flooding in many tropical and subtropical coastal areas because of their strong structures. Mangroves reduce waves and storm surges, and the roots of Mangroves protect the coastline against erosion and stabilizing the soil [35]. Furthermore, Mangroves survive in extreme environmental conditions and salty water. Because of all these benefits and the suitable Omani coastlines' favorable situation to grow Mangroves forests, it seems Mangroves forests are an environmentally friendly approach to protect the coastal zones against inland flooding, especially during tropical cyclones. The Sur port coastal flood characteristics have evaluated in two scenarios, including with and without Mangroves.

In this research, a Mangroves forest along the Sur port Shoreline was considered by determining a local Manning coefficient and the Mangroves forest's width. Figure 11 shows the assuming location of the Mangroves along the Sur port shoreline in the simulations. The Manning's coefficient (M) for open Mangroves in the coupled model was considered to be 20 $m^{1/3}/s^1$ [36], and the width of Mangroves was assigned as 90 m.

Figure 12a shows the spatial map of flood characteristic for inundation depth for the mitigation flood scenario with Mangroves. The maximum inundation all over the computational domain is almost less than 1 m in this scenario. The flow velocity pattern for the storm event is presented in Figure 12b. The maximum flow velocity for the mitigation flood scenario with Mangroves varies all over the study area, with its maximum magnitude being less than 0.5 m/s.

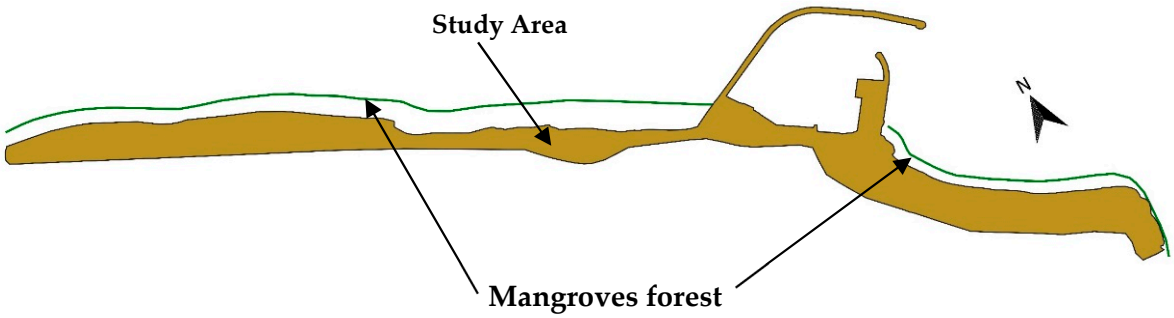

Figure 11. Schematic assumption Mangroves forest location in the model.

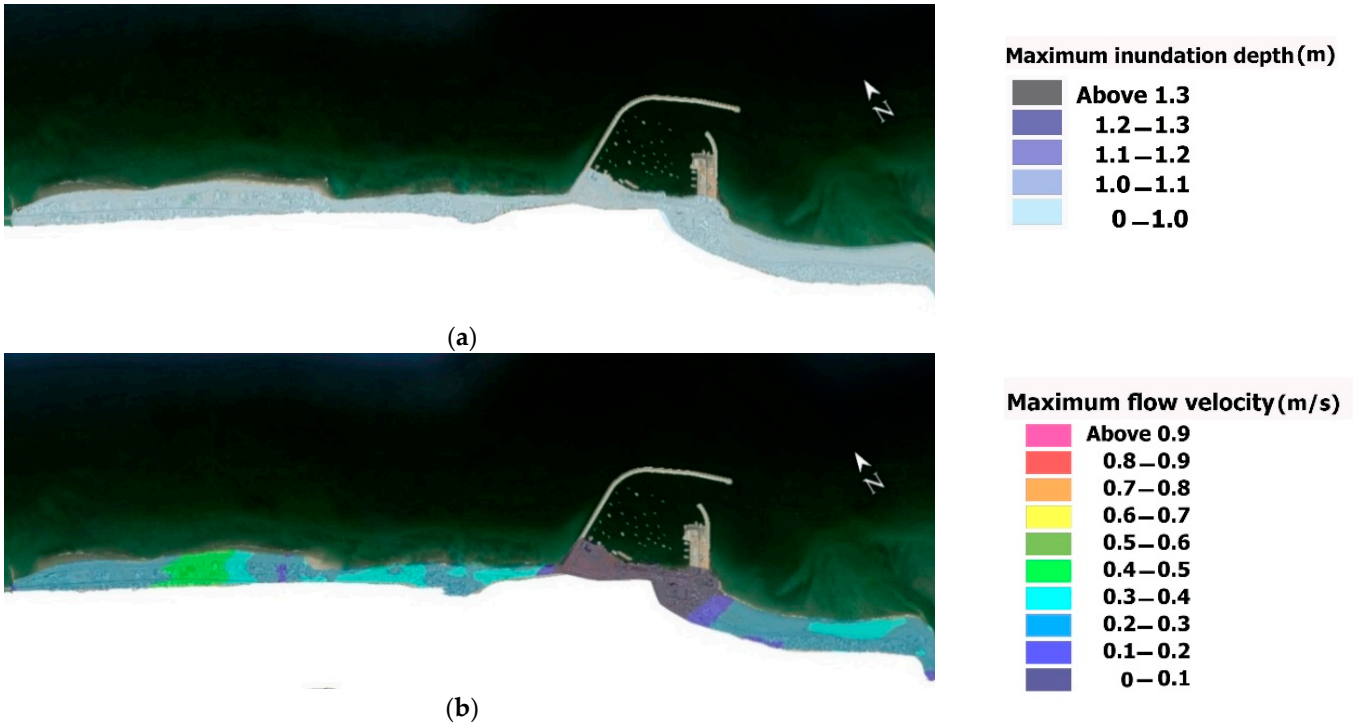

Figure 12. (**a**) Maximum inundation depth. (**b**) Maximum flow velocity in the study area according to the mitigation flood scenario model with Mangroves.

The flood hazard map, according to the Table 5, are plotted in Figure 13 for the mitigation flood scenario model with Mangroves. As shown in Figure 13, for this scenario, approximately 50% of the coast is assigned to the medium-risk class and 50% to the low-risk. By assuming the effect of Mangroves in the study area, the high-risk area almost removes completely. However, both medium and low-risk zones increase in the study area. The area with a low-risk to life is located mostly in the central and eastern parts of the model where the rubble mound breakwater is situated. The medium-risk to life areas exist mostly in the western parts of the coast, while some parts of the east coast are in medium-risk to life class.

Figure 13. Flood hazard map in the study area according to the mitigation flood scenario model with Mangroves.

5. Conclusions

Tropical cyclones are a serious threat to human lives and properties in coastal areas, which cause high destructive effects in these zones. Evaluating new approaches to protect and reduce cyclone's destructive impacts on habitats and properties is an important issue in coastal engineering and management. This study investigates the risk of floods due to the Gonu cyclone in the Sur port. Moreover, the impact of an assumption Mangroves forest as a flood risk reduction approach on the flood characteristics (inundation and flow velocity) is evaluated considering two scenarios, including with and without Mangroves forest along the shoreline. For this purpose, the coupled MIKE 21/3 HD/SW (hydrodynamic/spectral wave) model was simulated. Furthermore, the Young and Sobey, Holland and Rankine analytical vortex models were used to generate the wind and pressure fields during the Gonu cyclone passage. The following conclusions can be drawn:

- The analytical vortex models well captured the wind and pressure field during the storm event. However, the ECMWF ERA5 data did not accurately capture the wind and pressure field due to the proximity of the Gonu cyclone track to the study area. However, the ECMWF ERA5 data are accurate enough in non-cyclonic weather conditions.
- The storm surge near the Sur shore achieved its peak value of 0.44 m (by the Rankine vortex model). While the maximum surge in the normal condition was almost less than 0.1 m. This indicates that the Gonu cyclone led to a significant rise in seawater level that caused inland flooding. Meanwhile, it seems that there are no significant differences among the results of storm surge from different analytical vortex models.
- Maximum inundation depth occurs along the shoreline over the central part of the study area with the values ~1.3 m for the flood scenario without Mangroves. Moreover, in this scenario, for most of the western part of the model, the inundation depth increases up to ~1.1 m, while breakwater affects the inland flooding. The maximum inundation depth in the eastern part of the model is approximately less than 1 m.
- The maximum inundation all over the computational domain is almost less than 1 m for the flood scenario with Mangroves.
- The maximum flow velocity varies all over the study area with its maximum magnitude of more than 0.9 m/s for the flood scenario without Mangroves. While for the flood scenario with Mangroves, the maximum flow velocity is less than 0.5 m/s.
- The flood hazard map shows that 5% of the coast is at high-risk, 49% is at medium-risk, and 46% is at low-risk class for the flood scenario without Mangroves.
- By applying Mangroves as flood risk reduction, the flood hazard map shows that the high-risk area almost removes completely. However, medium and low-risk zones increase by 50% and 50%, respectively.
- The eastern part of the coast of Sur port seems to be well protected by the breakwater. While most parts of the west coast are unprotected and exposed to damage from storms and cyclones.

- Impact of large flood in urban and critical facilities and infrastructure can be reduced by timely and correct action before a disastrous storm, so managers and governments should be considered appropriate methods to mitigate cyclones' destructive effects. The use of artificial mangrove forests as an environmentally friendly method of protecting the coast can be an effective way to protect the Sur port against climate change and extreme environmental conditions.

Author Contributions: Conceptualization, M.B.-D. and M.S.-B.; methodology, M.B.-D., M.S.-B. and A.G.; software, M.B.-D. and M.S.-B.; validation, M.B.-D., M.S.-B. and A.G.; formal analysis, M.B.-D. and M.S.-B.; investigation, M.B.-D., M.S.-B. and A.G.; resources, M.B.-D. and M.S.-B.; data curation, M.B.-D., M.S.-B. and A.G.; writing-original draft preparation, A.M. and M.A.L.-Y.; writing-review and editing, S.A.; supervision, A.G., A.M. and M.A.L.-Y. All authors have read and agreed to the published version of the manuscript.

Funding: This research received no external funding.

Institutional Review Board Statement: Not applicable.

Informed Consent Statement: Not applicable.

Data Availability Statement: Not applicable.

Acknowledgments: Not applicable.

Conflicts of Interest: The authors declare no conflict of interest.

References

1. Bergillos, R.J.; Rodriguez-Delgado, C.; Medina, L.; Iglesias, G. Coastal cliff exposure and management. *Ocean Coast. Manag.* **2020**, *198*, 105387. [CrossRef]
2. Bergillos, R.J.; Rodriguez-Delgado, C.; Cremades, J.; Medina, L.; Iglesias, G. Multi-criteria characterization and mapping of coastal cliff environments: A case study in NW Spain. *Sci. Total Environ.* **2020**, *746*, 140942. [CrossRef]
3. Bergillos, R.J.; Ortega-Sánchez, M. Assessing and mitigating the landscape effects of river damming on the Guadalfeo River delta, southern Spain. *Landsc. Urban Plan.* **2017**, *165*, 117–129. [CrossRef]
4. Mojtahedi, A.; Beiragh, M.S.; Farajpour, I.; Mohammadian, M. Investigation on hydrodynamic performance of an environmentally friendly pile breakwater. *Ocean Eng.* **2020**, *217*, 107942. [CrossRef]
5. Emanuel, K. Increasing destructiveness of tropical cyclones over the past 30 years. *Nature* **2005**, *436*, 686. [CrossRef] [PubMed]
6. Henderson-Sellers, A.; Zhang, H.; Berz, G.; Emanuel, K.; Gray, W.; Landsea, C.; Holland, G.; Lighthill, J.; Shieh, L.; Webster, P.; et al. Tropical cyclones and global climate change: A post-IPCC assessment. *Bull. Am. Meteor. Soc.* **1998**, *79*, 19–38. [CrossRef]
7. Golshani, A.; Taebi, S. Numerical modeling and warning procedure for Gonu super cyclone along Iranian Coastlines. In Proceedings of the Solutions to Coastal Disasters 2008 Conference, Turtle Bay, Oahu, NI, USA, 13–16 April 2008; pp. 268–275.
8. Dibajnia, M.; Soltanpour, M.; Nairn, R.; Allahyar, M. Cyclone Gonu: The most intense tropical cyclone on record in the Arabian Sea. In *Indian Ocean Tropical Cyclones and Climate Change*; Springer: Dordrecht, The Netherlands, 2010; pp. 149–157.
9. Banan-Dalalian, M.; Shokatian-Beiragh, M.; Golshani, A.; Mojtahedi, A.; Lotfollahi-Yaghin, M.A. Study of the Effect of Gonu Tropical Cyclone on the Oman Coastlines Inland Flooding (Case Study: The Coastline of Sur). In Proceedings of the 2nd International Conference on Oceanography for West Asia (RCOWA 2020), Tehran, Iran, 16–17 September 2020; p. 11.
10. Fritz, H.M.; Blount, C.D.; Albusaidi, F.B.; Al-Harthy, A.H.M. Cyclone Gonu storm surge in Oman. *Estuar. Coast. Shelf Sci.* **2010**, *86*, 102–106. [CrossRef]
11. Khaniki, A.; Meshkati, A.; Bidokhti, A. Tropical cyclone Induced waves in the Chabahar Bay area. In Proceedings of the 11th MIC, Kish Island, Iran, 9–11 November 2009. (In Persian).
12. Mashhadi, L.; Zaker, N.H.; Soltanpour, M.; Moghimi, S. Study of the Gonu Tropical Cyclone in the Arabian Sea. *J. Coast. Res.* **2013**, *31*, 616–623. [CrossRef]
13. Bakhtiari, A.; Allahyar, M.R.; Jedari Attari, M.; Haghshenas, S.A.; Bagheri, M. Modeling of Last Recent Tropical Storms in the Arabian Sea. *J. Mar. Sci. Eng.* **2018**, *1*, 58–66.
14. Wang, Z.; DiMarco, S.F.; Stössel, M.M.; Zhang, X.; Howard, M.K.; Vall, K.D. Oscillation responses to tropical Cyclone Gonu in northern Arabian Sea from a moored observing system. *Deep Sea Res. I Oceanogr. Res. Pap.* **2012**, *64*, 129–145. [CrossRef]
15. Jayakrishnan, P.R.; Babu, C.A. Study of the oceanic heat budget components over the Arabian Sea during the formation and evolution of super cyclone, Gonu. *Atmos. Clim. Sci.* **2013**, *3*, 282–290. [CrossRef]
16. Allahdadi, M.N.; Chaichitehrani, N.; Allahyar, M.; McGee, L. Wave spectral patterns during a historical cyclone: A numerical model for cyclone Gonu in the northern Oman Sea. *Open J. Fluid Dyn.* **2017**, *7*, 131–151. [CrossRef]
17. Allahdadi, M.N.; Chaichitehrani, N.; Jose, F.; Nasrollahi, A.; Afshar, A.; Allahyar, M. Cyclone-generated storm surge in the northern Gulf of Oman: A field data analysis during cyclone Gonu. *Am. J. Fluid Dyn.* **2018**, *8*, 10–18.

18. Al-Awadhi, T. The Use of RS and GIS to Evaluate the Effects of Tropical Cyclones: A Case Study from A'Seeb, Muscat after GONU Cyclone. In Proceedings of the 1st WMO International Conference on Indian Ocean Tropical Cyclones and Climate Change, Muscat, Oman, 8–11 March 2009; p. 95.
19. Jedari, M.; Bakhtiari, A.; Dibajnia, M.; Golshani, A.S.; Shafieefar, M. *Study Reports of Monitoring and Modelling Studies of Markan Coastlines*; Ports and Maritime Organization (PMO): Tehran, Iran, 2017.
20. Siahsarani, A.; Khaniki, A.K.; Bidokhti, A.A.A.; Azadi, M. Sensitivity analysis of the numerical aspect of the SWAN for the tropical cyclone wave simulations in the Gulf of Oman. *Arab. J. Geosci.* **2020**, *13*, 1–14. [CrossRef]
21. DHI. *MIKE 21 Spectral Wave Model User Guide*; DHI: Hørsholm, Denmark, 2014.
22. DHI. *MIKE 21 Flow Model FM User Guide*; DHI: Hørsholm, Denmark, 2014.
23. Morin, V.; Warnitchai, P.; Weesakul, S. Storm surge hazard in Manila Bay: Typhoon Nesat (Pedring) and the SW monsoon. *Nat. Hazards* **2016**, *81*, 1569–1588. [CrossRef]
24. Dong, S.; Stephenson, W.J.; Wakes, S.; Chen, Z.; Ge, J. Meso-scale Simulation of Typhoon Generated Storm Surge: Methodology and Shanghai Case Study. *Nat. Hazards Earth Syst.* **2017**. [CrossRef]
25. DHI. *MIKE 21 Cyclone wind Generation Tool Scientific Documentation*; DHI: Hørsholm, Denmark, 2014.
26. Young, I.R.; Sobey, R.J. *The Numerical Prediction of Tropical Cyclone Wind-Waves*; Department of Civil & Systems Engineering, James Cook University of North Queensland: Townsville, QLD, Australia, 1981.
27. Holland, G.J. An Analytic Model of the Wind and Pressure Profiles in Hurricanes. *Mon. Weather Rev.* **1980**, *108*, 1212–1218. [CrossRef]
28. Rankine, W.J.M. *A Manual of Applied Mechanics*; Charles Griffin and Company: London, UK, 1872.
29. Nash, J.E.; Sutcliffe, J.V. River flow forecasting through conceptual models part I—A discussion of principles. *J. Hydrol.* **1970**, *10*, 282–290. [CrossRef]
30. Ritter, A.; Munoz-Carpena, R. Performance evaluation of hydrological models: Statistical significance for reducing subjectivity in goodness-of-fit assessments. *J. Hydrol.* **2013**, *480*, 33–45. [CrossRef]
31. McLachlan, A.; Fisher, M.; Al-Habsi, H.N.; Al-Shukairi, S.S.; Al-Habsi, A.M. Ecology of sandy beaches in Oman. *J. Coast. Conserv.* **1998**, *4*, 181–190. [CrossRef]
32. Chow, V.T. *Open-Channel Hydraulics*; McGraw-Hill: New York, NY, USA, 1959.
33. Kaiser, G.; Scheele, L.; Kortenhaus, A.; Løvholt, F.; Römer, H.; Leschka, S. The influence of land cover roughness on the results of high resolution tsunami inundation modeling. *Nat. Hazards Earth Syst. Sci.* **2011**, *11*, 2521–2540. [CrossRef]
34. Priest, S.J.; Wilson, T.; Tapsell, S.M.; Penning-Rowsell, E.C.; Viavattene, C.; Fernandez Bilbao, A. *Building a Model to Estimate Risk to Life for European Flood Events*; Project Report; HR Wallingford: Wallingford, UK, 2007.
35. Liu, H.; Zhang, K.; Li, Y.; Xie, L. Numerical study of the sensitivity of mangroves in reducing storm surge and flooding to hurricane characteristics in southern Florida. *Cont. Shelf Res.* **2013**, *64*, 51–65. [CrossRef]
36. Machineni, N.; Sinha, V.S.; Singh, P.; Reddy, N.T. The impact of distributed landuse information in hydrodynamic model application in storm surge inundation. *Estuar. Coast. Shelf Sci.* **2019**, *231*, 106466. [CrossRef]